NAVAL POSTGRADUATE SCHOOL
MONTEREY, CALIFORNIA

THESIS

AN ELECTRON BACKSCATTER DIFFRACTION ANALYSIS OF THE MICROSTRUCTURE OF PURE ALUMINUM PROCESSED BY EQUAL-CHANNEL ANGULAR PRESSING

by

Shannon D. Terhune

December 1998

Thesis Advisor: Terry R. McNelley

Approved for public release; distribution is unlimited.

REPORT DOCUMENTATION PAGE

Form Approved OMB No. 0704-0188

1. AGENCY USE ONLY *(Leave blank)*	2. **REPORT DATE** December 1998	3. **REPORT TYPE AND DATES COVERED** Master's Thesis

4. TITLE AND SUBTITLE
AN ELECTRON BACKSCATTER DIFFRACTION ANALYSIS OF THE MICROSTRUCTURE OF PURE ALUMINUM PROCESSED BY EQUAL-CHANNEL ANGULAR PRESSING

5. FUNDING NUMBERS

6. AUTHOR(S) Shannon Derek Terhune

7. PERFORMING ORGANIZATION NAME(S) AND ADDRESS(ES)
Naval Postgraduate School
A. Monterey CA 93943-5000

8. PERFORMING ORGANIZATION REPORT NUMBER

9. SPONSORING/MONITORING AGENCY NAME(S) AND ADDRESS(ES)

10. SPONSORING/MONITORING AGENCY REPORT NUMBER

11. SUPPLEMENTARY NOTES. The views expressed in this thesis are those of the author and do not reflect the official policy or position of the Department of Defense or the U.S. Government.

12a. DISTRIBUTION/AVAILABILITY STATEMENT
Approved for public release; distribution is unlimited.

12b. DISTRIBUTION CODE

13. ABSTRACT *(maximum 200 words)*

Equal-channel angular (ECA) pressing is a promising method to achieve refinement of grain size to 1.0 μm or less for aluminum and its alloys. Computer-aided electron backscatter diffraction (EBSD) analysis of high purity aluminum (99.99%) which had been subjected to one pass, four passes, and twelve passes through an ECA die was performed. Grain and subgrain size and boundary misorientation distributions during such large-strain deformation processing were of particular interest. A texture was present after one pressing and the boundary misorientation distribution had a peak at 5^0 – 10^0 although boundaries were present in all misorientation ranges. Fine equaixed grains were achieved after twelve passes through the ECA die, accompanied by random orientation and misorientation distributions

14. SUBJECT TERMS
Equal-Channel Angular Pressing, Electron Backscatter Diffraction, Grain Refinement, Sub-Micrometer Grain Refinement, Massive Deformation, Plastic Deformation, Deformation Banding, Boundary Misorientation, Preferred Misorientation Angle.

15. NUMBER OF PAGES
62

16. PRICE CODE

17. SECURITY CLASSIFICATION OF REPORT	18. SECURITY CLASSIFICATION OF THIS PAGE	19. SECURITY CLASSIFICATION OF ABSTRACT	20. LIMITATION OF ABSTRACT
Unclassified	Unclassified	Unclassified	UL

NSN 7540-01-280-5500

Standard Form 298 (Rev. 2-89)
Prescribed by ANSI Std. 239-18 298-102

Approved for public release; distribution is unlimited

AN ELECTRON BACKSCATTER DIFFRACTION ANALYSIS OF THE MICROSTRUCTURE OF PURE ALUMINUM PROCESSED BY EQUAL-CHANNEL ANGULAR PRESSING

Shannon Derek Terhune
Lieutenant, United States Navy
B.S.E.E., Virginia Military Institute, 1992

Submitted in partial fulfillment of the
requirements for the degree of

MASTER OF SCIENCE IN MECHANICAL ENGINEERING

from the

NAVAL POSTGRADUATE SCHOOL
December 1998

Author: Shannon Terhune
Shannon D. Terhune

Approved by: T R McNelley
Terry R. McNelley, Thesis Advisor

T R McNelley
Terry R. McNelley , Chairman
Department of Mechanical Engineering

ABSTRACT

Equal-channel angular (ECA) pressing is a promising method to achieve refinement of grain size to 1.0 μm or less for aluminum and its alloys. Computer-aided electron backscatter diffraction (EBSD) analysis of high purity aluminum (99.99%) which had been subjected to one pass, four passes, and twelve passes through an ECA die was performed. Grain and subgrain size and boundary misorientation distributions during such large-strain deformation processing were of particular interest. A texture was present after one pressing and the boundary misorientation distribution had a peak at 5^0 – 10^0 although boundaries were present in all misorientation ranges. Fine equaixed grains were achieved after twelve passes through the ECA die, accompanied by random orientation and misorientation distributions.

TABLE OF CONTENTS

I. INTRODUCTION

Grain size refinement is generally recognized for producing improved combinations of strength and toughness in engineering alloys. Recent studies have shown that extreme refinement can be achieved by imposing very large plastic strains using techniques such as equal-channel angular (ECA) pressing [Ref. 1-4]. Submicrometer and even nanometer grain sizes have been reported [Ref. 5]. This thesis is a report on the grain boundary character associated with grain refinement resulting from room temperature ECA pressing of pure aluminum. In this chapter, the roles of grain size and grain boundary character on strength are discussed, followed by a review of the current understanding of the recrystallization phenomenon following deformation of metals.

In general, five different mechanisms are recognized for contributing to the strength of metallic materials. All of these (strain hardening, grain size, solid-solution alloying, precipitation hardening, and dispersion strengthening) involve restricting dislocation motion in some way [Ref. 6], however, only strain hardening and grain refinement are applicable to pure metals as well as alloys. Reduced ductility and toughness generally accompany increasing strength, except when strengthening is accomplished by the grain size mechanism. Consequently, grain refinement is especially desirable in metals.

Many theories have been developed to explain the physics of strengthening by grain size refinement. All of these consider that the grain boundary is a barrier to

dislocation motion. Hall and Petch [Ref. 7] proposed that, at the initiation of plastic deformation, dislocation pile-ups form at the grain boundaries in grains favorably oriented for slip. These pile-ups produce areas of high stress concentration where the dislocations penetrate the grain boundaries into less favorably oriented grains, which results in the occurrence of general yielding. The Hall-Petch relationship is

$$\sigma_y = \sigma_0 + kD^{-1/2} \qquad (1)$$

where σ_y is the tensile yield stress, σ_0 is a frictional stress to move dislocations within grains, and D is the grain diameter. Cottrell [Ref. 7] proposed an improvement on this theory. He addressed the unlikely case of dislocations moving directly from grain to grain by proposing that the stress concentrations instead initiate slip at Frank-Read (F-R) sources in neighboring grains, where these F-R sources lie adjacent to the grain boundary [Ref . 7]. The resulting equation is similar in form to (1), but includes a factor the distance from the grain boundary to the F-R source at which slip is initiated in the adjacent grain. Theories by Li and Conrad [Ref. 7] additionally consider dislocation motion through the grain interior instead of limiting their scope exclusively to the vicinity of the grain boundary. Dislocations must overcome both thermal (short range) and athermal (long range) barriers, however, the resulting relationship for the strength is identical in form to equation (1). Reference 7 provides detailed discussions of the derivations of these models. Others have proposed that grain boundary discontinuities themselves are the dislocation sources and they, not the pile-ups, cause the dislocation arrays.

In all of these models the grain boundaries are assumed to be effective barriers to dislocation motion. Thus, the boundaries are assumed to be high-angle in nature where the lack of lattice registry across the boundary plane provides a strong barrier to dislocation motion through the boundary plane. Low-angle boundaries consisting of dislocation arrays would not be as effective as barriers because of a relatively high degree of lattice registry in the boundary plane. Therefore, the term D is taken to represent a grain size and not a subgrain size. However, specific requirements for grain boundaries are yet to be established. It is now possible to obtain statistically significant quantitative measures of grain boundary character, i.e. misorientation angle. Availability of this relatively new data will greatly facilitate the design of processing methods to achieve required engineering properties.

Since all of the conventional theories of grain size strengthening predict $\sigma \alpha D^{-1/2}$ grain size dependence, the influence of grain refinement can be estimated. It can be shown that a typical 50 μm grain size contributes about 5 kg/mm^2 to the yield strength of a typical alloy [Ref. 8]. Thus, decreasing the grain size by an order of magnitude increases this contribution to strength by about 3 times; as a result, extrapolation to more substantial increases in yield strength require refinement to grain sizes in the submicron range [Ref. 8].

Refining the grain size of engineering alloys may be accomplished several ways, depending on the material selected. Heat treatment methods involving controlled thermal treatments have been used for many years on alloys of iron and titanium that undergo the phase transformations exhibited by these metals during cooling. For most other alloys,

including nickel, copper, and aluminum, the only available methods are those where the material undergoes deformation followed by recrystallization.

During deformation, strain energy is stored in the form of dislocations. Recovery and recrystallization are driven by the release of this energy during subsequent annealing. The recrystallization process is often thought of as a nucleation and growth process where the formation of new grain boundaries is supported by the release of this stored strain energy. However, Doherty [Ref. 9] has reviewed the standard model from kinetic theory and concluded that stored strain energy is insufficient for this purpose. He notes that the energy barrier to new grain formation can be written as

$$\Delta G^* = (\alpha\gamma^3/\Delta G_v^2) f(\cos\vartheta) \qquad (2)$$

where α is $16\pi/3$ for spheres, γ is the grain boundary energy, ϑ is a contact angle for nucleation on a pre-existing interface, and $f(\cos\vartheta)$ is between 0.1 and 0.5. Values for the dislocation line energy and dislocation density typical of a deformed metal result in ΔG_v = 1 MPa. This low value in conjunction with typical high-angle boundary energy γ = 0.5 J/m^2 gives a resulting ΔG^* value that is so large, 10^5kT, that even at temperatures above half the melting temperature the theory predicts no new grain formation. This is unquestionably contrary to observed results [Ref. 9]. Essentially, there is not enough stored strain energy available to overcome the effects of the surface term in equation 2.

This problem of theory may be resolved by recognizing that the nuclei of the new grains do not form through atom-by-atom addition to an embryo, instead they consist of small cells or subgrains already present in the deformed material. This is consistent with the observation that the orientations of new grains do not tend to be random, but often

have orientations inherited from the prior, deformed state. This has been recognized in the experimental work of Hatherly [Ref. 10] and Haasen [Ref. 11].

Complex dislocation configurations resulting from severe deformation in metals give a structure in the deformed state which is not fully understood. It is recognized that plastic deformation results in the generation and motion of dislocations to allow the material to accommodate the externally imposed shape change without fracturing. These dislocation configurations develop during large strain deformation processing. They include isolated dislocations, planar arrays and cellular structures. In cellular structures, which form by dislocation reaction, the dislocations are incorporated into the cell walls causing lattice misorientation. These misorientations may be low-angle or high-angle in nature depending on the processing history.

Recent work [Ref. 12-14] on superplastic processing of aluminum alloys has shown that the grain boundary misorientations of Supral 2004, in the superplastically enabled state, are already present in a cellular dislocation structure which develops during the final cold rolling of the material. Also, it has been shown that deformation banding occurs during deformation processing [Ref. 15,16]. Band formation is a process of grain subdivision. The bands form when the lattice rotates in different orientations in adjacent regions. The importance of deformation banding has long been recognized [Ref. 17]. Its occurrence during rolling may allow certain regions in the material, which contain bands, to deform in plane strain even though plane strain conditions may not be met within the band. The possibility of such band formation during ECA pressing operations will be considered in this work.

Finally, the problem of microstructural control isn't fully solved with grain refinement by recrystallization processing. Subsequent grain growth must be controlled if a new finer grain size material is to be maintained. Usually, grain growth occurs during annealing according to the relation given in Reference 6,

$$D = Ct^n \qquad (3)$$

where D is the grain size, C is a constant and n is a time constant. For steels, controlling the exposure to elevated temperatures may work well due to the high melting temperature of Fe. For aluminum, which has a much lower melting temperature, grain growth presents a more severe problem, especially for pure aluminum because it may even recrystallize at room temperature. Methods to limit the rate of grain boundary migration include the introduction of alloying elements as well as dispersed particles.

II. BACKGROUND

A. WHY EQUAL-CHANNEL AREA PRESSING

To achieve desired grain size reduction in aluminum some form of deformation processing and recrystallization treatment is required. It is generally recognized that increased prior strain (beyond a threshold value) during deformation generally will result in finer grains during a subsequent recrystallization treatment. To impart strains large enough to produce grains of diameter on the order of a micrometer in pure aluminum, processes such as redundant forging [Ref .18,19], high pressure torsional loading [Ref. 20], inert gas condensation [Ref. 21], high energy ball milling [Ref. 22], sliding wear [Ref . 23], and equal-channel angular (ECA) pressing [Ref 1-4] are required.

The concept of ECA pressing was developed and first demonstrated by Segal [Ref. 24] and possesses several distinct advantages. First, it is relatively low in cost and straightforward in application. Second, for pure aluminum it can be done at room temperature. This allows for control of grain growth during recrystallization treatments. Third, the cross sectional area remains constant throughout the process. This is very significant because it allows for repeated passes through the ECA die in order to impart large amounts of strain but without a corresponding reduction in cross-sectional area [Ref . 25].

Because of these attractive characteristics, ECA pressing offers significant potential as an industrial technique to produce desired microstructural refinement. Several laboratories throughout the world have begun to publish results of experiments on ECA processing. These facilities include Monash University in Clayton, Victoria,

Australia; Kyushu University and Fukuoka University of Education in Fukuoka, Japan; Ufa State Technical University in Ufa, Russia; and The University of Southern California in Los Angeles, California, to name a few. In the current study, Dr. Terence G. Langdon supplied samples that had been processed in the University of Southern California's Department of Materials Science and Engineering laboratory.

B. EQUAL-CHANNEL AREA PRESSING APPARATUS

ECA pressing consists of extruding a billet of material through a die of constant cross-sectional area but which has two die channels that intersect at an angle Φ. For the material of this study, the geometry of the processing equipment is shown schematically in Figure 2.1. [Ref. 25]

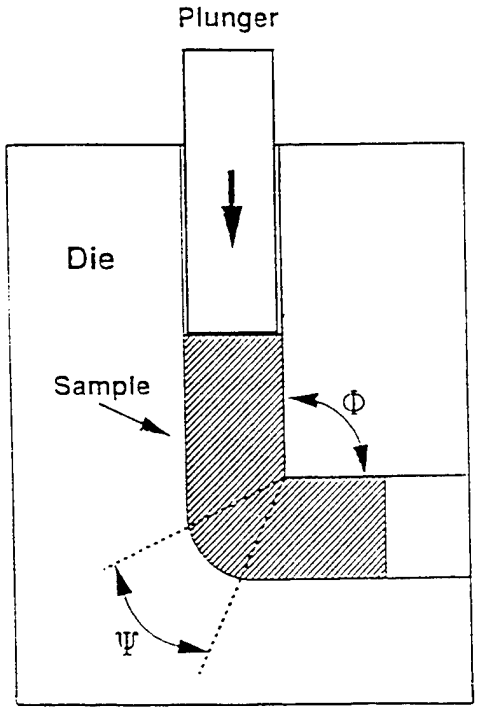

Figure 2.1. Schematic of ECA pressing apparatus. $\Phi = 90°$ and $\Psi = 20°$

The die is made from 2 pieces of tool steel, machined to obtain the geometry of the die channel shown, which are bolted together to form the pressing facility. Iwahashi and coworkers [Ref. 26] have calculated the strain for the ECA pressing through such a die to be given by equation (4)

$$\varepsilon_N = N / (3)^{1/2} [\, 2 \cot (\phi/2 + \psi/2) + \psi \quad \mathrm{cosec}(\phi/2 + \psi/2)] \qquad (4)$$

where N is the number of pressings [Ref. 26]. Here, the angle $\Phi = 90°$; the angle $\psi = 20°$ has been determined by experimental trial and error [Ref. 27] to be necessary for smooth operation of the plunger without lodging an aluminum billet in the die. For these values, equation (5) becomes $\varepsilon_N = 1.055N$; i.e., the material will experience a true plastic strain of approximately unity for each passage through the die [Ref. 26].

There are several geometrical considerations in conducting microstructural analysis of material processed by ECA pressing. First, there are three orthogonal planes, X, Y and Z as indicated by the schematic of Fig. 2.2. In this work, the Y plane was examined in all cases. Also, after the initial pass through an ECA die, a sample may be rotated about its longitudinal axis. Iwahashi, et al. [Ref . 26] have discussed the various possibilites; their route A (illustrated in Fig. 2.3), in which the sample is not rotated between pressings, was that used for the processing of the material in this study. Studies wherein the sample has been rotated between pressings, and wherein the angle Φ has been varied, have been published recently [Ref. 25, 26] .

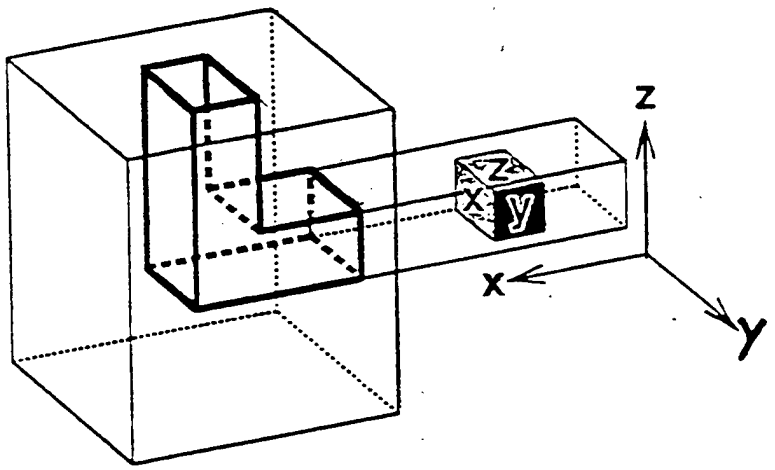

Figure 2.2. The three orthogonal planes x, y, and z in the ECA apparatus.

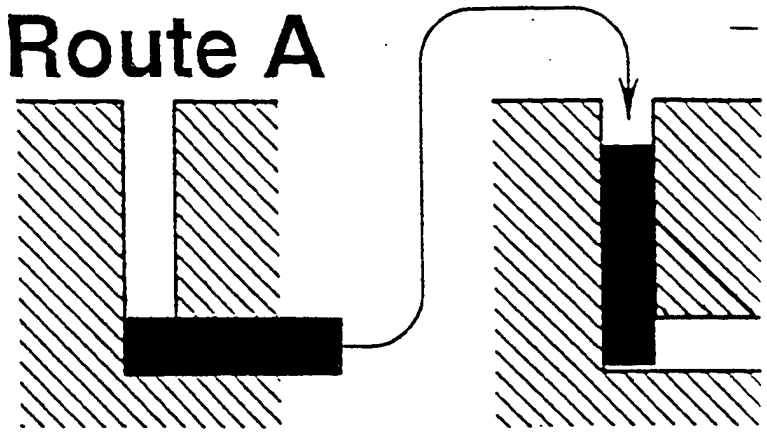

Figure 2.3. Route A. No sample rotation between pressings.

The material of the present study was pure aluminum (99.99%) which had been machined from an as-received plate to fit the die. The samples had an initial grain size of about 0.5 μm before pressing. The machined billets were lubricated with a MoS_2 and pressed at a speed of about 0.75 in/sec at room temperature with a 10 ton press [Ref. 28].

C. OBJECTIVES OF THE STUDY

In recent studies by Langdon and colleagues [Ref. 26] pure aluminum, with an initial grain size on the order of a 0.5 μm, was reported to be refined to an apparent grain size of about 1.0 μm after 10 pressings. It was also found that, as successive pressings were performed, the grain structure evolved from one consisting mainly of subgrains of low apparent misorientation to an apparently recrystallized state with high angle boundaries after 10 pressings [Ref . 26]. However, these conclusions about the boundary structure were obtained by use of selected area diffraction methods in a transmission electron microscope (TEM). The TEM analysis utilized a 13 μm aperture so that the diffraction data were obtained from a large number of (sub)grains. The drawback of this approach is it does not permit direct assessment of the grain-to-grain misorientations. For this purpose, grain specific orientation measurements are needed.

Electron backscatter diffraction (EBSD) methods in a scanning electron microscope (SEM) allows individual grain orientations to be measured by using the electron beam of the SEM as a probe. Computer-aided diffraction pattern analysis methods have been coupled with EBSD to provide a method of rapid acquisition of large numbers of grain orientations in a pre-determined pattern. This method allows the ready

determination of grain boundary character in terms of the distribution of misorientation angles. A general description of EBSD in the SEM has been given by Randle et al. [Ref. 29]; more specific discussion on the methods developed in this laboratory and utilized in this study have been provided elsewhere [Ref. 30].

The objective of the present investigation was to obtain microtexture data for pure aluminum processed by ECA pressing according to Langdon's route A, and to assess the evolution of the microtextures and the grain boundary misorientation distributions as a function of strain during repetitive pressing operations. It was also intended to assess these data in light of recent advances in the understanding of deformation microstructures and recrystallization. Supplementary objectives included the assessment of the possible role of deformation banding during ECA straining.

III. EXPERIMENTAL METHODS

A. SAMPLE PREPARATION FOR EBSD ANALYSIS

Three samples of pure (99.99%) ingot metallurgy aluminum , which had been pressed at room temperature through the ECA die described in the previous chapter, were selected for evaluation. The samples had been pressed one, four, or twelve times with corresponding strain values of $e_N \sim 1.1$; 4.2; or 12.7. Prior to examination sectioning was done both perpendicular to and parallel with the axis of the pressed samples in order to obtain a flat, rectangular specimen representing the Y plane. (Figure 3.1) illustrates the specific geometry.

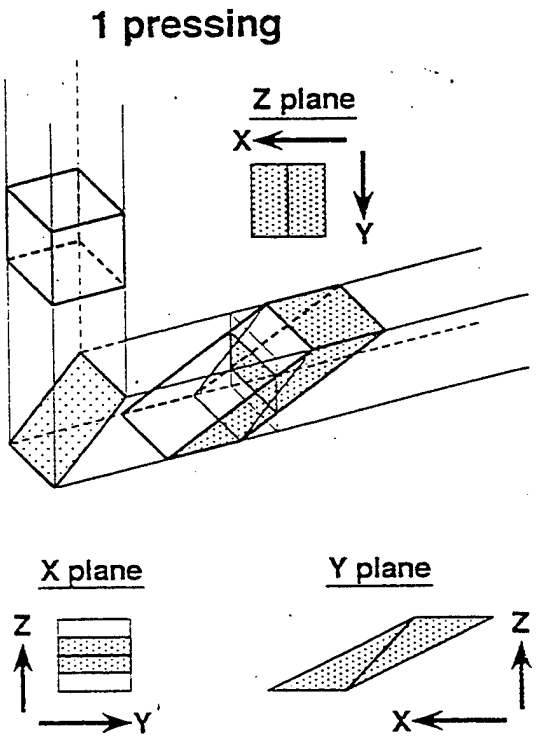

Figure 3.1. Schematic illustration of the deformation in the X, Y, and Z planes [Ref. 26]

Sectioning was accomplished using a Buehler low-speed diamond saw operating at 400 rpm. Samples were cut to the approximate dimensions of 1cm x 1.4cm x 0.5cm. Figure 3.2 details the geometry of the sectioning.

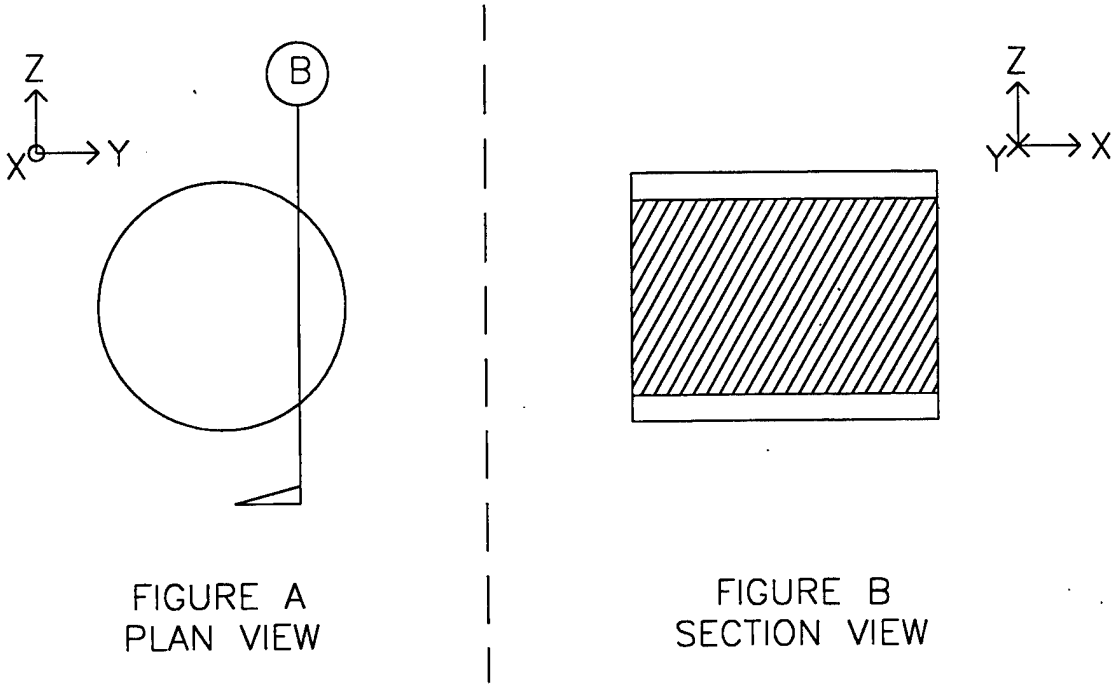

Figure 3.2. Geometry of sample sectioning

To remove the resulting distortion generated on the sectioned surface of the aluminum, the samples were mechanically polished using successively finer grits according to the schedule outlined in (Table 3.1).

Step	*Polishing Medium*	*Grit*	*Grit diameter*	*time (min)*	*rpm*
1	carbide paper	500	30 mm	1	300
2	carbide paper	1000	18 mm	2	300
3	carbide paper	2400	10 mm	3	300
4	carbide paper	4000	5 mm	3	300
5	diamond spray	-	6 mm	10	240
6	diamond spray	-	1 mm	15	240
7	colloidal silica	-	0.5 mm	3	500

Table 3.1. Mechanical polishing operation

Subsequent electropolishing of the sample was required. Several different combinations of solutions, voltages, currents, and polishing times were tried until a successful procedure was developed. Electropolishing proved to be the most challenging and most critical step in achieving acceptable results with the SEM. It should be noted that the EBSD patterns were formed within only 30nm of the sample surface, and both surface oxide layers and residual strains severely degraded diffraction pattern quality. Removal of all surface layers and polishing-induced mechanical damage was necessary. The chemical solutions used included 70% methanol - 30% nitric acid and 90% butoxyethanol - 10% hydrochloric acid at voltages ranging from 7 volts to 30 volts and times of 2 to 20 minutes. Each run with these reagents was unsuccessful with the pure aluminum.

Next, a solution of 80% ethanol - 20% perchloric acid (according to Ref. 2) was tried, utilizing 15 volts and 50 mA for 4 minutes; this gave a satisfactory result. After final adjustments, a combination of 80% ethanol - 20% perchloric acid, 8 volts DC, and a

current density of 0.1 amps/cm^2 in a -50°C methanol bath for 10 minutes was used for electropolishing. Samples were masked using lacquer to provide stop off, so that only an area of about 1.5 mm^2 would be exposed to the electropolishing solution.

Extreme care was taken in order to prevent contamination of the sample surface after electropolishing. The steps taken included using a methanol rinse which had been stored in a glass container rather than a polyethylene bottle. Also, because an oxide layer can easily form on the surface of the pure aluminum resulting in poor pattern quality in the microscope, care was taken to avoid extreme temperature fluctuations of the sample. The methanol used to rinse the perchloric acid from the sample was kept below 0°C and only cool, forced air was used to dry the sample.

B. ELECTRON BACKSCATTER DIFFRACTION

The discovery of electron diffraction from crystal lattices, by Davisson and Germer's 1927 experiment with slow electrons and single crystal nickel, was the first evidence of DeBroglie's 1924 theory of the particle-wave duality of the electron. It was then shown that electron diffraction followed the same Bragg's law which had been formulated for X-ray diffraction [Ref. 31]. The relation is

$$n\lambda = 2d \sin\theta \qquad (5)$$

where n is the order of diffraction, λ is the wavelength of electrons (0.007 nm for 20 keV electrons [Ref. 31]), d is the interplanar spacing, and q is the diffraction angle.

Electron diffraction has the advantage over X-ray diffraction of giving surface crystal structure due to the more shallow penetration of electrons than X-rays [Ref. 30].

For pure aluminum in a SEM at 20 KV the penetrating distance is 20-30 nm [Ref. 32]. Analysis of the aluminum samples in the present work utilized electron backscatter pattern (EBSP) methods with the SEM in conjunction with both computer hardware and software developed by TexSem Laboratories, Inc. (Figure 3.3) represents the facility at the Naval Postgraduate School. The major components include a Topcom SM-510 scanning electron microscope, a fiber-optic charge-coupled device LTC216 low-light camera mounted to a phosphor lens, a model 852 camera control unit, and a Silicon Graphics INDY workstation with installed Orientation imaging software .

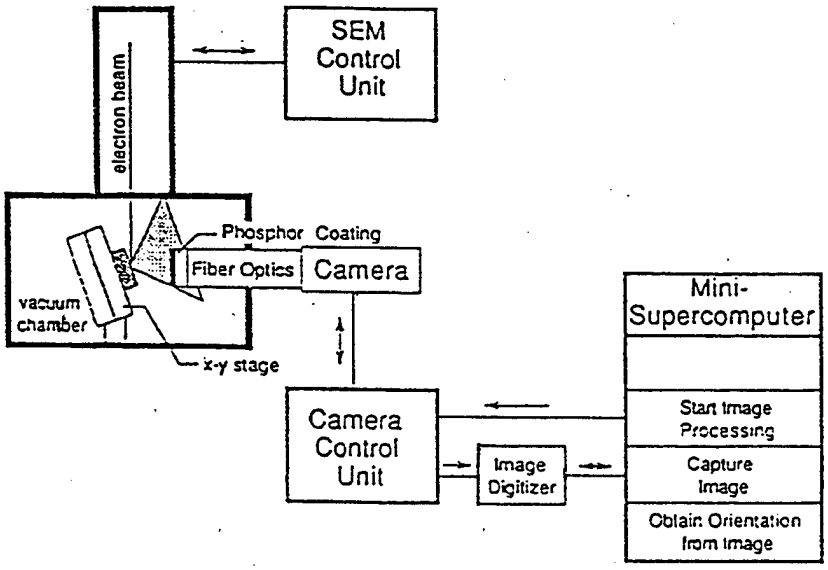

Figure 3.3. Schematic of an EBSD system's major components [Ref. 30]

Backscatter electron diffraction patterns were a result of incident electrons being scattered by the crystal lattice according to Bragg's law. The diffracted electrons produced a Kikuchi line pattern on a screen mounted in the microscope specimen chamber. Figure 3.4 depicts the formation of an EBSP.

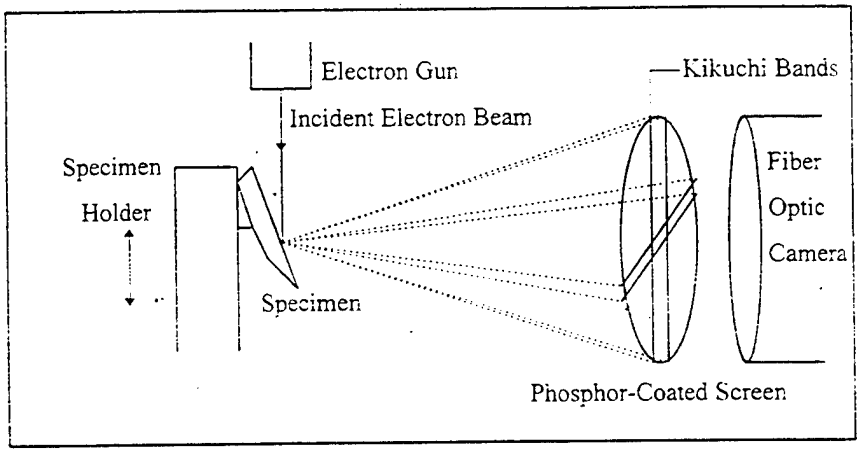

Figure 3.4. Schematic of the formation of an EBSP [Ref.32]

By analysis of the pattern geometry, the crystal lattice orientation of the diffraction region on the sample surface was determined. The Orientation Imaging Microscopy (OIM) software automatically indexed these patterns. A pictorial representation of this process is shown in Figure 3.5. Because each grain in the material had its own crystal orientation it also had its own diffraction pattern. The software enabled the capture and analysis of the diffraction patterns. Analysis of a pattern provided three Euler angles which uniquely described the lattice orientation in relation to

a set of default axes assumed in the software. These Euler angles were stored as part of an *.ang data file (Figure 3.6). Specific functions of the APR software used for this study included determination of the misorientation angle between adjacent grains, the calculation, and the plotting of misorientation histograms and pole figures.

C. PROCEDURE FOR DATA COLLECTION

In practice, each sample was placed in a holder designed to maintain a 70° angle between the sample normal and the electron beam of the SEM. This angle provided the optimum signal-to-noise ratio in the resulting Kikuchi patterns. These patterns were formed on a phosphor screen inside the SEM chamber and were detected by a low-light camera. The image of the Kikuchi pattern was captured by a camera control unit (CCU), which integrated the camera signal, digitized the resulting pattern, and then transmitted it to an INDY workstation for analysis with the OIM software. The software captured the pattern and assigned Euler angle data to it. After the data for a given grain was stored, the beam was translated to the neighboring grain along the intended traverse, and the process was repeated. As a rule of thumb, at least 400 successive patterns needed to be captured to get a good statistical representation of texture.

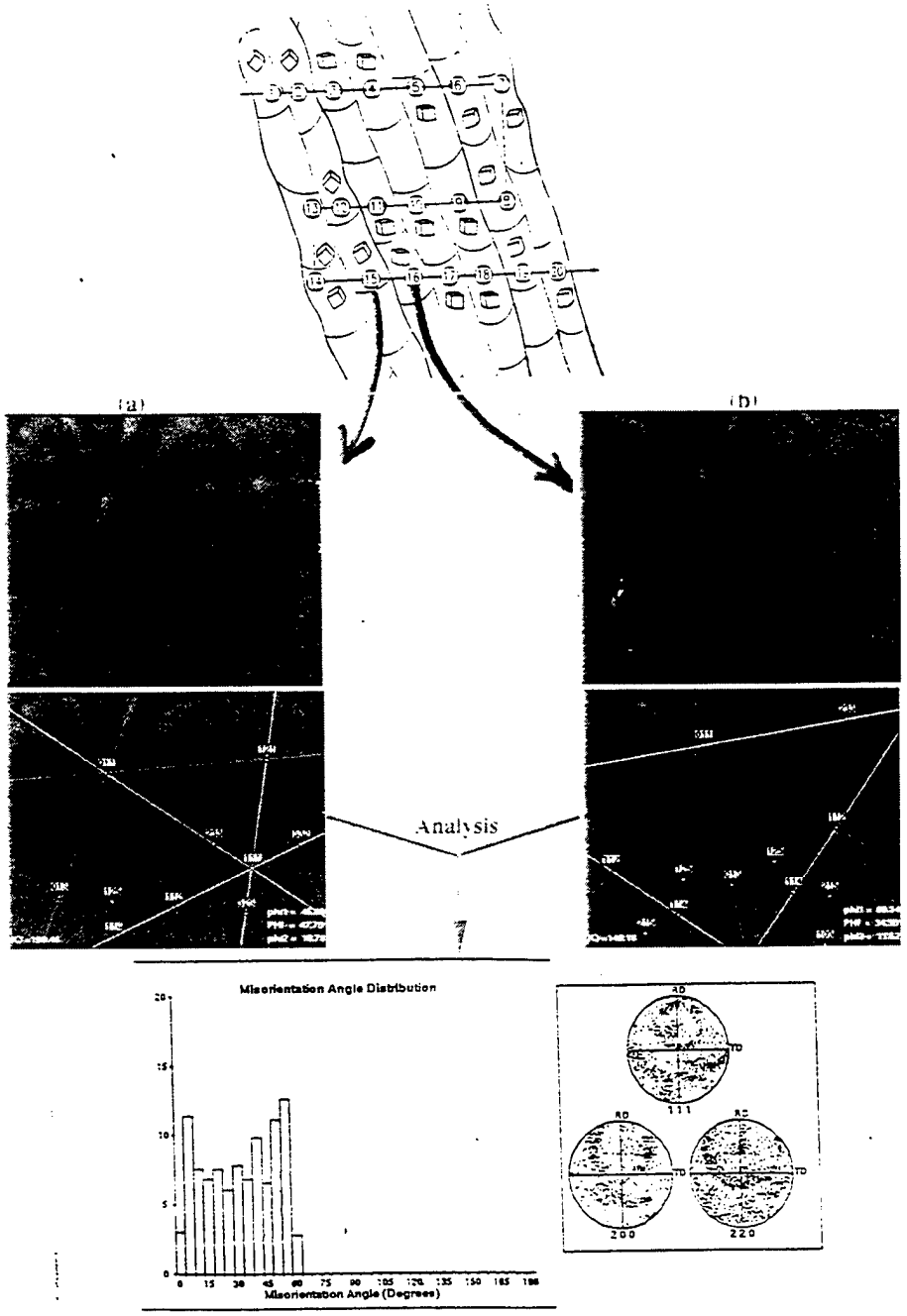

Figure 3.5. Schematic of the formation of an EBSP orientation. Two sequentially captured patterns are collected and indexed [Ref. 30].

```
# WorkDirectory         /usr/people/naval
# OIMDirectory          /usr/OIM
# x-star                296
# y-star                175
# z-star                430
# WorkingDistance       20
# MaterialName          fcc_generic
# Symmetry              43
# LatticeConstants      4.000 4.000 4.000  90.000  90.000  90.000
# NumberFamilies        4
# hklFamilies            1  1  1
# hklFamilies            2  0  0
# hklFamilies            2  2  0
# hklFamilies            3  1  1
#
   1.933    1.376    5.794     0.000     0.000   24.3  0.000 01y2ndrun1
   3.938    0.188    4.487     0.000     0.000   14.3  0.000 01y2ndrun2
   4.363    0.229    3.886     0.000     0.000   16.1  0.000 01y2ndrun3
   0.201    0.285    0.640     0.000     0.000   16.6  0.000 01y2ndrun4
   4.363    0.229    3.886     0.000     0.000   15.0  0.000 01y2ndrun5
   2.410    0.602    5.646     0.000     0.000   17.2  0.000 01y2ndrun6
   1.814    1.091    6.191     0.000     0.000   14.9  0.000 01y2ndrun7
   0.216    0.359    0.752     0.000     0.000   26.5  0.000 01y2ndrun8
   0.337    0.291    0.645     0.000     0.000   25.9  0.000 01y2ndrun9
   3.631    0.478    4.101     0.000     0.000   16.2  0.000 01y2ndrun10
   3.609    0.534    4.195     0.000     0.000   14.5  0.000 01y2ndrun11
   0.548    0.591    0.811     0.000     0.000   12.5  0.000 01y2ndrun12
   3.536    0.519    4.276     0.000     0.000   16.0  0.000 01y2ndrun13
   3.536    0.701    4.520     0.000     0.000   15.7  0.000 01y2ndrun14
   3.631    0.478    4.101     0.000     0.000   12.8  0.000 01y2ndrun15
   3.403    0.530    4.553     0.000     0.000   14.2  0.000 01y2ndrun17
   3.609    0.534    4.195     0.000     0.000   15.7  0.000 01y2ndrun19
   3.574    0.509    4.218     0.000     0.000   20.9  0.000 01y2ndrun20
   2.175    0.947    5.787     0.000     0.000   16.4  0.000 01y2ndrun21
   2.318    0.606    5.726     0.000     0.000   14.2  0.000 01y2ndrun22
   3.356    0.521    4.612     0.000     0.000   15.3  0.000 01y2ndrun23
   0.346    0.386    0.791     0.000     0.000   17.4  0.000 01y2ndrun24
   0.047    0.310    0.775     0.000     0.000   15.9  0.000 01y2ndrun25
   4.378    0.282    3.885     0.000     0.000   16.4  0.000 01y2ndrun26
   0.825    0.620    0.671     0.000     0.000   26.9  0.000 01y2ndrun27
   1.972    1.319    6.103     0.000     0.000   15.2  0.000 01y2ndrun28
   1.997    1.329    6.080     0.000     0.000   13.4  0.000 01y2ndrun29
   3.609    0.534    4.195     0.000     0.000   15.1  0.000 01y2ndrun30
   3.609    0.534    4.195     0.000     0.000   14.5  0.000 01y2ndrun31
   0.774    0.585    0.610     0.000     0.000   12.3  0.000 01y2ndrun32
```

Figure 3.6. Excerpt of a *.ang data file

Immediately following the electropolishing step, the sample was placed in the 70° tilted holder which was mounted in the TOPCON 510 SEM chamber. The working distance was set to 20 mm, the accelerating voltage to 20 kV, and the spot size to 12 giving an electron probe diameter of about 100nm. The spot size was smaller than the

grains in question, otherwise overlapping patterns could have resulted. The image was then focused at 500X and a background image was captured for later subtraction while actual patterns were taken. After switching to spot mode, a diffraction pattern was observed on the monitor. The image was then "captured." This meant that the CCU integrated 16 real time frames, subtracted the background, and displayed the resulting image of the pattern on the monitor [Ref. 32]. Next, the APR software digitized the pattern, indexed it (after proper calibration for fcc), and saved it for later analysis. Then, the CCU was switched back to real time and the electron "spot" was moved until the pattern changed. This indicated that a grain boundary had been crossed. As noted above, from this point the whole process was repeated to obtain at least 400 grain orientations.

The beam was traversed in raster pattern as shown schematically in (Figure 3.7). A certain amount of forethought was necessary to determine the raster pattern to be followed. A long horizontal path was chosen because the working distance remained constant. Small (ten successive pattern captures) traverses were conducted in the vertical direction because, for each movement in the vertical direction, the working distance changed due to the 70° tilt of the sample. For each successive long horizontal traverse, the APR system was recalibrated for the new working distance.

The *.ang file generated by the APR software included the Euler angles (ϕ_1, Φ, ϕ_2), the image quality index, empty reserved columns for software upgrades, and the number sequence name of the saved pattern. The Euler angles reference the axis of the pressed sample as up and down, and the image quality is the measure of the contrast difference between the pattern lines and the empty spaces between lines.

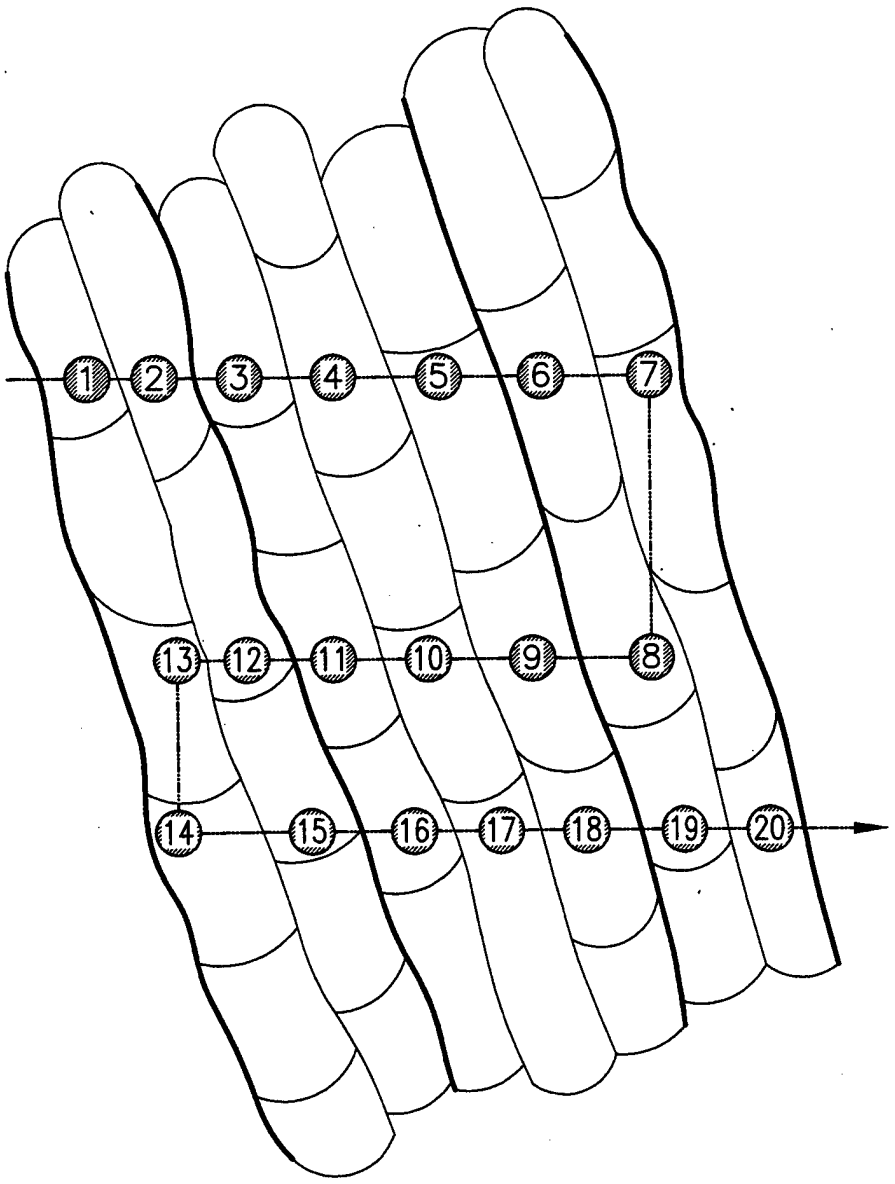

Figure 3.7. Schematic of raster pattern beam was traversed

A mean linear spacing which is analogous to a mean linear intercept for the grain size, was determined by the following method: a portion of the raster pattern was started at the edge of the SEM monitor and ended at the opposite edge. The number of spots or patterns captured was counted for the traverse across the screen. The distance across the screen was displayed on the monitor, so a mean spacing between patterns equalled the number of patterns over the distance traversed. This was calculated for comparison to results obtained by conventional imaging methods in the SEM and TEM.

D. TRANSMISSION ELECTRON MICROSCOPY

The twelve pass sample was observed in the TEM with the goal of obtaining imaging of the sample. This particular processing route had no previous imaging in publication, so the imaging of the this sample was completed.

Again, samples were sectioned using a Buehler low-speed diamond saw operating at 400 rpm. Specimens were sectioned to an approximate thickness of 50 μm and were thinned to 15 μm using 1000 grit wet paper on a wheel rotating at 300 rpm. Next, 2400 grit paper was then used to thin to 10 μm followed by 4000 grit to a final thickness of 8 μm or less. Next, 3 mm discs were punched out and subsequently thinned to perforation using a twin jet polishing unit. The solution used was identical to that of the SEM analysis, 80% ethanol and 20% perchloric acid at a temperature of -50°C, 7 volts and 200mA.

IV. RESULTS AND DISCUSSION

EBSP measurements were taken to obtain microtexture data which provided information on the texture, grain boundary misorientation and separation distance between successive crystallographic orientations. TEM observations were conducted on a single sample that had not been imaged in previous work. Together, these new data provided insight into the development of the grain boundaries in this material during processing to large strains by ECA pressing.

A. INFLUENCE OF PRESSING ON MICROSTRUCTURE

An extensive investigation into the evolution of microstructure during ECA pressing of pure aluminum, identical to samples studied in this research, was previously reported by Iwahashi, et al. [Ref. 26]. TEM results were reported on this route A material following one pass and four passes (conditions studied in the present work) as well as additional conditions. For this material following one ECA pass, the micrographs showed a cellular microstructure consisting of elongated, parallel bands consisting mostly of subgrains. Selected area diffraction (SAD) results suggested that the boundaries were of relatively low misorientation although no quantitative misorientation measurements were reported. The bands tended to be aligned with the axis of the pressed sample, indicative of a fibrous microstructure which had formed as a result of large plastic deformation. Figure 5.1 is adapted from Ref. 26 and illustrates a subgrain size of about 1 μm in the short dimension (the radial direction in the pressing) and about 3 μm in the longitudinal dimension.

A similar, elongated structure was seen in samples that had experienced up to 6 repeated pressing operations. The elongated dimension was reduced from 3 μm to 2 μm through six successive pressings, but the short dimension remained essentially constant. After 10 pressings a nearly equiaxed microstructure had become apparent and selected area diffraction measurements were interpreted as evidence for the development of high-angle boundaries at this large strain.

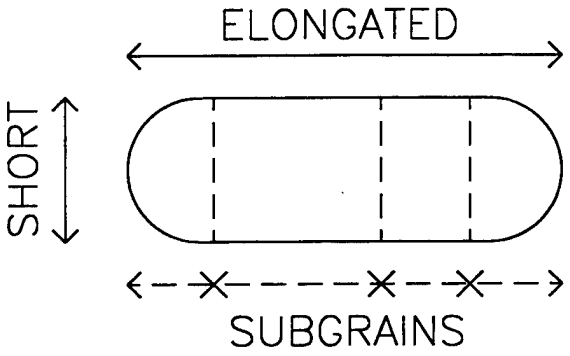

Figure 5.1. Schematic of elongated grain/subgrain, illustrating the typical dimensions of the fiber-like structure. [Ref. 26]

A schematic representation of an elongated, banded structure, representative of those in samples experiencing one or four pressings, is shown in Figure 5.2. Superimposed on this is a raster pattern illustrating the traverse through the microstructure utilized in the EBSD analysis of the present work. The elongated bands may represent regions of similar orientation . This is shown schematically with the cube drawings, intended to represent the lattice orientation, of Figure 5.2. In such a structure it

would be expected that similar orientations would be encountered while traversing in a direction parallel to the bands, and more pronounced orientation changes would be seen while traversing perpendicular to the bands.

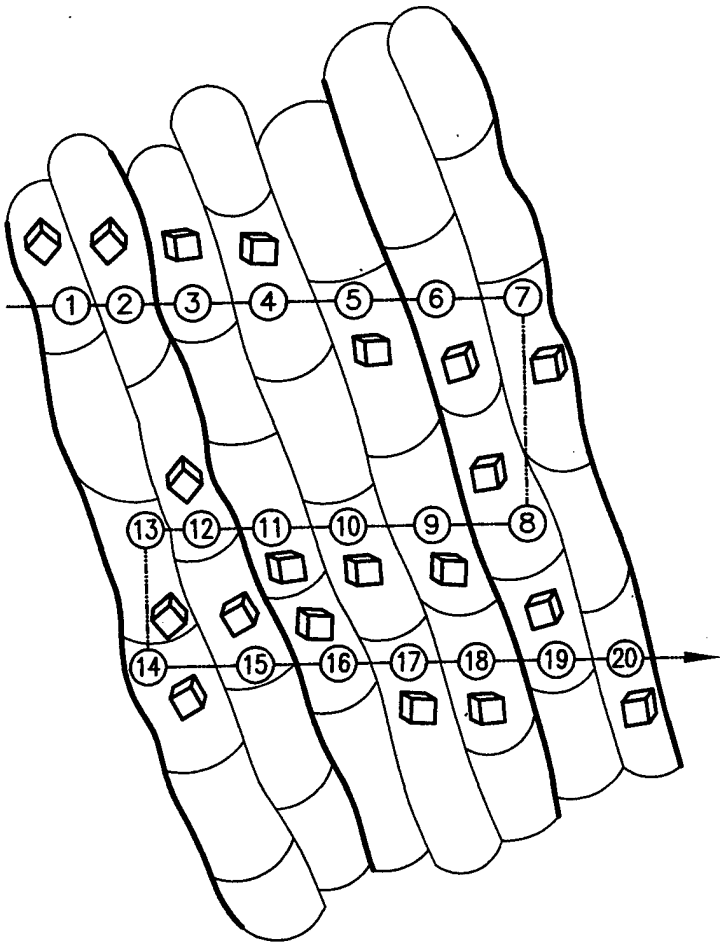

Figure 5.2. Schematic of microstructure for the 1 and 4 pass specimen showing the elongated, banded structure with the superimposed raster pattern used for EBSD analysis.

The 12 pressings billet was examined in the TEM for this study because no microscopy results had been previously reported on this particular sample. Figure 5.3 is a TEM micrograph illustrating an equiaxed and highly refined microstructure. The (sub)grain size is about 1 μm, a value consistent with earlier results for material that had experienced 10 pressings [Ref. 5]. This observation supports the assertion that the microstructure reaches a 'steady state' at some point beyond the sixth pressing operation. In the event that the boundaries evident in this micrograph are high-angle in nature, this also indicates the potential of ECA pressing to reduce the original 500 μm grain size of this pure aluminum material to about 1 μm while maintaining a constant cross-sectional area in the material.

Figure 5.3. TEM micrograph of the sample processed by route A through 12 pressing operations (y plane)

B. POLE FIGURES

EBSD data in the form of approximately 400 sequential orientations was acquired for samples that had experienced one, four or twelve ECA pressing passes utilizing processing route A. The orientation data may be represented in the form of pole figures. The pole figures presented in Figures 5.4 and 5.5 were computed from the orientation data obtained from the respective samples and are plotted as discrete data. In Figure 5.4 the pole figures have been plotted such that the Normal Direction (ND) in each figure corresponds to the axis of the as-pressed sample. Then, the Transverse Direction (TD) (the designation is that provided by the APR software, which assumes a rolled sheet) is oriented as the normal to the Y face of the sample and RD is then orthogonal to ND and TD and, furthermore, is parallel to the pressing direction.

It is evident that after one pressing there is a weak <110> fiber texture. This is seen most prominently in the {220} pole figure in the form of a high concentration of orientations near the center of the figure. There is also a diffuse ring of orientations in this figure, consistent with rotational symmetry about the axis of the as-pressed sample, although the population of orientations is not uniform around this ring. Diffuse rings are also apparent in the {111} and {200} figures but a non-uniform distribution around these rings is also apparent.

The <110> fiber texture becomes more distinct after four pressings. This is most apparent, again, in the {220} pole figure. The ring of orientations located 60° from ND exhibits a more uniform distribution of orientations around the fiber axis. However, the corresponding rings in the {111} pole figure (at 35.3° and 90°from ND), and in the {200}

pole figure (at 45°and 90°), do not exhibit a uniform distribution of orientations. Careful examination of these latter pole figures suggests a weak tendency for a <111> to be aligned with the TD, i.e. a <111> perpendicular to the Y plane of the pressed sample. It is especially noteworthy that continued pressing results in the elimination of texture by the 12th pressing operation. All three pole figures exhibit essentially random distributions of orientations in this processing condition. An alternative representation of the data may be obtained by a coordinate rotation wherein the axis of the as-pressed sample becomes aligned with the RD in these pole figure representations. The <110> fiber texture is now apparent in the high population of orientations along RD in the {220} pole figures for the one and four pressing samples. The rotational symmetry is now apparent in the form of bands of orientations ±30° from TD in the {220} figures; corresponding bands in the {111} and {200} pole figures do not exhibit uniform orientation distributions. Finally, the random nature of the texture after 12 pressings is apparent.

Wire textures in cold-drawn aluminum generally consist of a predominant <111> orientation with a weak <100> (<uvw> is parallel to the wire or fiber axis) [Ref 33]. Neither of these crystallographic orientations lies parallel to the axis of these ECA pressed samples; instead, <110> lies parallel to this direction. Few studies of texture or microtexture development during ECA pressing of metals have been published. Gibbs, et al. [Ref. 34] have reported X-ray texture data for nominally pure iron following ECA pressing using routes A, B and C. They conclude that route A should produce a texture similar to a rolled sheet where the plane of shear, as the billet passes through the die, becomes aligned parallel to the Z plane during a series of pressing operations. A fiber

fiber texture would be expected for route B where the sample is given alternating 90° rotations between successive pressings, subsequently leading to rotational symmetry.

The results of the current research do not support the conclusions of Gibbs, et al. [Ref. 34] regarding texture formation in relation to processing route. A distinct fiber texture is seen for this route A material based on 400 discrete orientation measurements. The alignment of <110> with the axis of the pressing becomes stronger between one and four pressing operations, but has disappeared after 12 pressings and the texture has become essentially random.

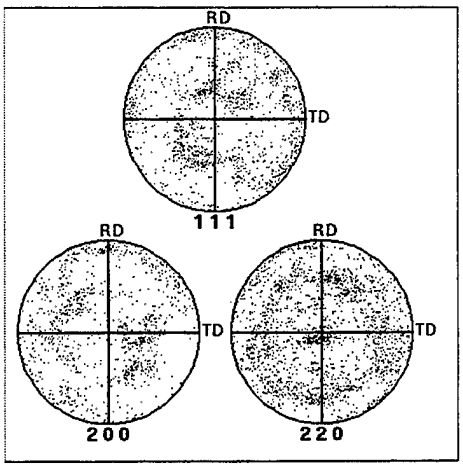

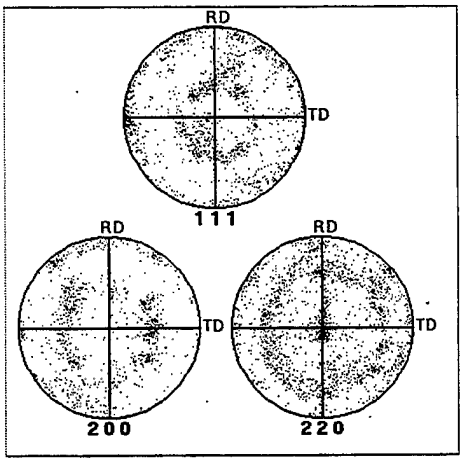

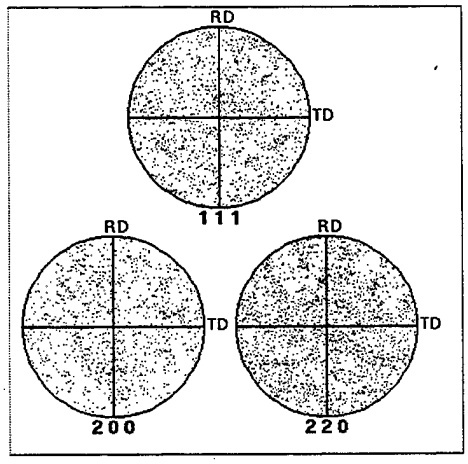

Figure 5.4 Pole figure data for one, four and 12 ECA passes. The ND is aligned with the axis of each pressing

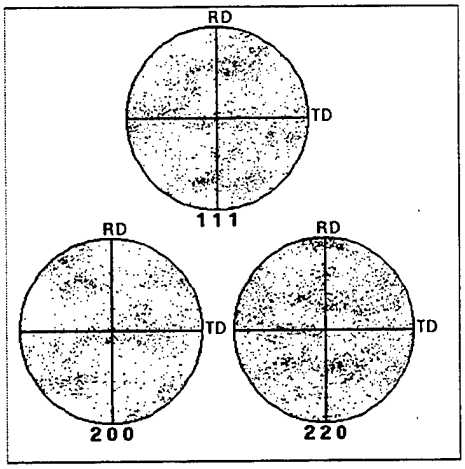

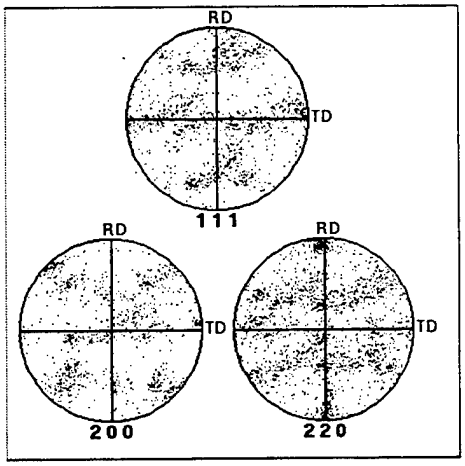

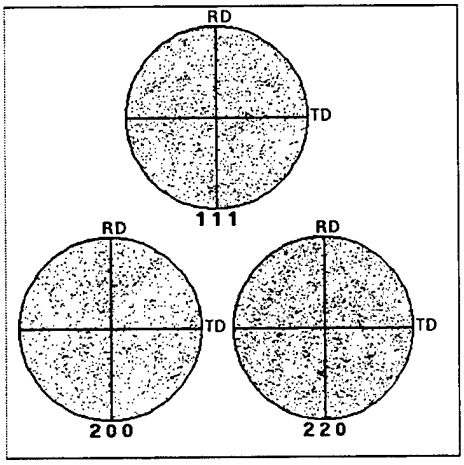

Figure 5.5 Pole figure data for one, four and 12 ECA passes. The RD is aligned with the axis of the pressings.

C. MISORIENTATION DATA

During data collection the individual grain orientations were obtained in succession. Thus grain-to-grain misorientations were calculated, using the APR software. This was accomplished automatically computing the minimum misorientation angle and corresponding rotation axis, and then bringing the lattice of neighboring grains into coincidence while considering crystal symmetry. With such a definition, the range of possible misorientation angles is 0° - 62.8° for a cubic material, and the data is represented in the form of histograms showing the relative population of boundaries in various misorientation bins within this range. In addition, the mean distance between grains was calculated as outlined in chapter III. The results of these calculations are that the grain size reduces to 2.1 μm after one pressing; 1.3 μm after four pressings; and 1.2 μm after twelve pressing passes through the die.

The grain-to-grain misorientation data generated for these samples is displayed in Figure (5.6). Such misorientation data for neighboring grains is generally referred to as *correlated* misorientation data in that the grains are always nearest neighbors. The histogram for the material after one pressing pass shows a bimodal distribution with boundaries present in all possible misorientation ranges. It is noteworthy that there is a peak in the distribution at 5° - 10°, and that about 48% of all boundaries are misoriented by less than 20°. A second, smaller peak is located at 45° - 50°. This indicates that even through grain refinement from 500 μm to 2.1 μm occurs during one pass, the structure is dominated by low angle boundaries which are less effective than random high angle boundaries in the obstruction of dislocation motion.

Following four pressing passes the grain size has decreased further to 1.3 μm, reflecting the large total strain introduced. The histogram again shows boundaries present in every misorientation range, but the distribution has shifted from one dominated by low-angle boundaries to a somewhat 'flatter' but still bimodal distribution. This data suggest a progressive increase in boundary misorientation due to accumulation of dislocations into boundaries during large-strain deformation processing.

For the sample that had experienced twelve ECA passes, an additional strain of about 8.0 had been accumulated, but there was only a slight further reduction in grain size, from 1.3 μm to 1.2 μm. Again, boundaries are present in all misorientation ranges but there is now a single peak in the histogram, located at 35° - 40°. This histogram is similar to the Mackenzie [Ref. 35] misorientation distribution for randomly oriented cubes. The probability density distribution for the Mackenzie distribution is shown in Figure 5.7. Such a distribution, in conjunction with the randomizing of texture, suggests that recrystallization has occurred during repetitive ECA pressing at room temperature.

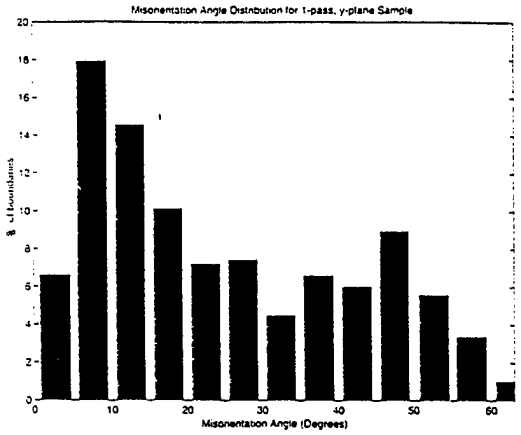

2.1 μm

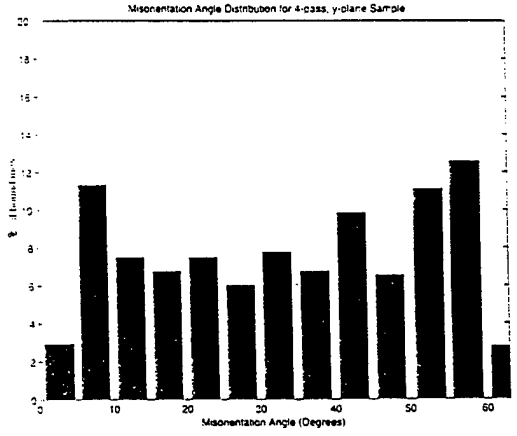

1.3 μm

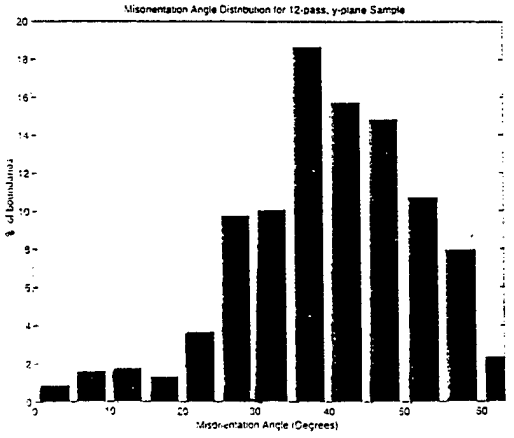

1.2 μm

Figure 5.6. The correlated misorientation distributions for samples after one, four and 12 ECA pressing passes.

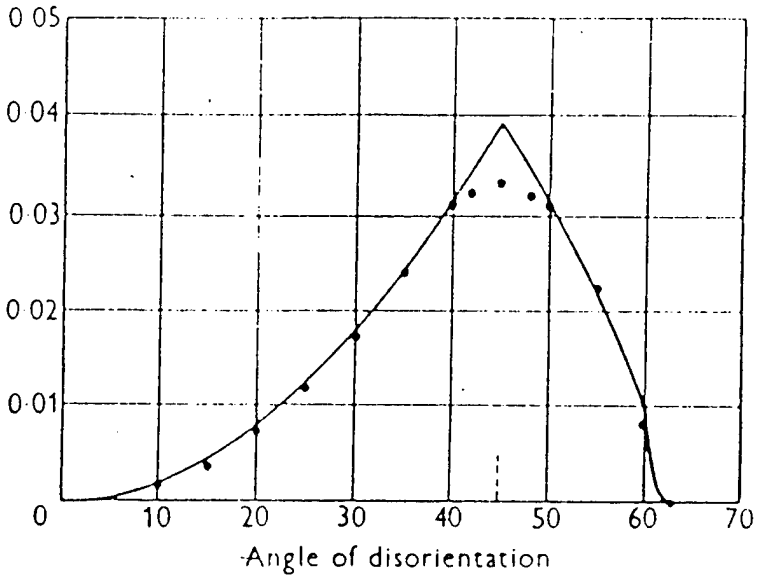

Figure 5.7. The Mackenzie probability density distribution for the misorientation of randomly oriented cubes. [Ref. 35]

D. UNCORRELATED DATA

The correlated misorientation distributions shown in Figure 5.6 are for adjacent grains. It is also possible to determine the misorientation of any one specific grain to all others in the assemblage; such a distribution is uncorrelated. Differences in the correlated and uncorrelated distributions may reflect grain-to-grain interactions during deformation

and annealing processes. Here, uncorrelated distributions were determined by means of the "C" computer program [Ref.36] summarized in Appendix A. Essentially, the program generated a new data file allowing comparison of each grain orientation to all others of the 400 grains in the data set.

Uncorrelated misorientation distributions corresponding to the correlated data of Figure 5.6 are shown in Figure 5.8. These distributions all exhibit a single peak (always at 45° - 50°), although the distributions differ somewhat in shape. In all cases, the uncorrelated distributions, which are based on texture alone, under predict the observed populations of low angle boundaries. The ratio of the correlated to the uncorrelated distributions is plotted in Figure 5.9. This representation emphasizes that the population of low-angle boundaries in one and four pass materials greatly exceeds that needed to accommodate orientation differences in the material, and also shows that the population of high-angle boundaries is lower than that predicted by texture alone. As processing strain increases, this ratio tends toward unity, although the number of low angle boundaries always exceeds the prediction based on texture. The overall trend is for an upward shift in misorientation of low-angle boundaries, which is consistent with the incorporation of dislocations into the boundaries during successive pressing operations.

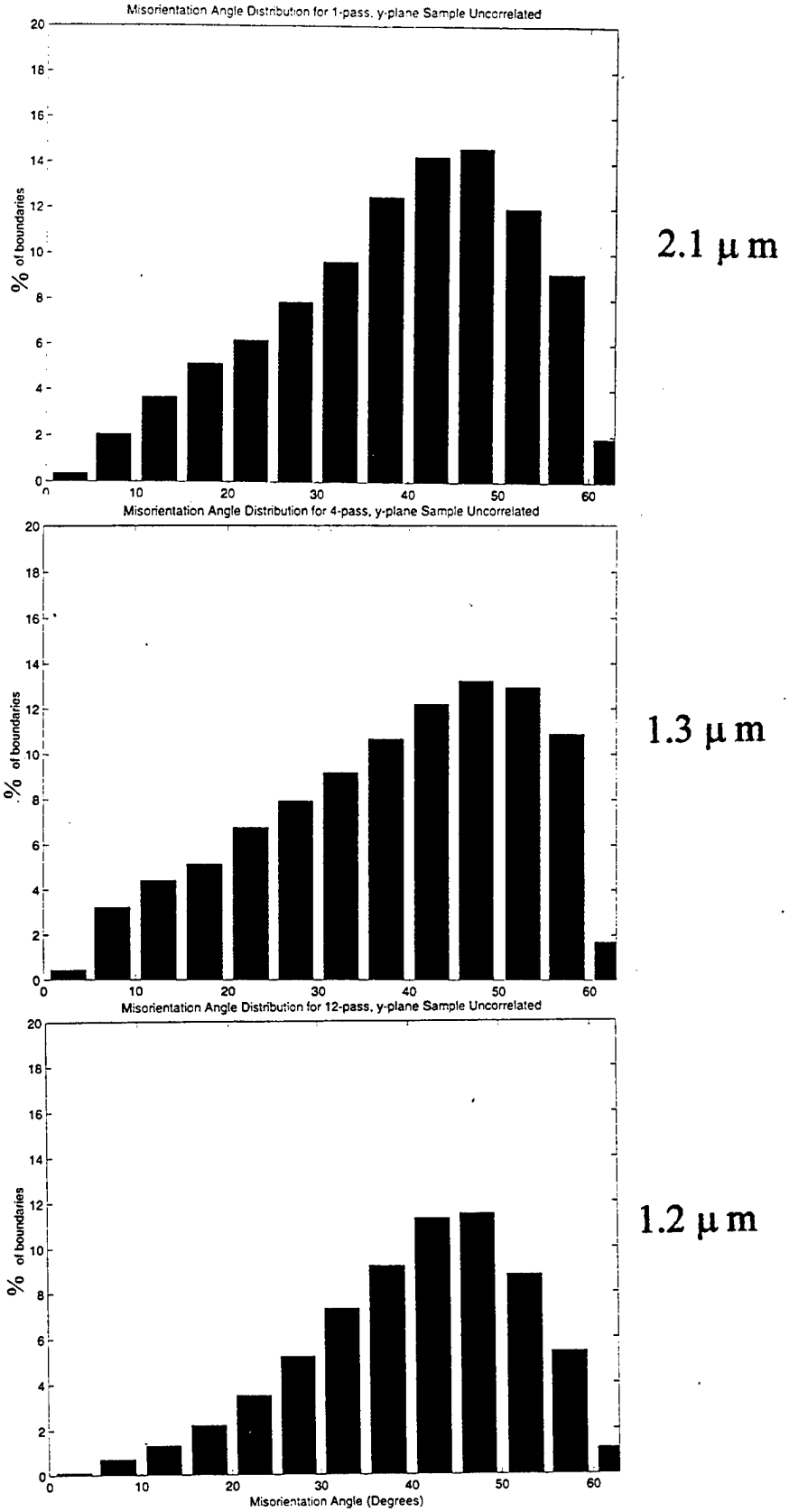

Figure 5.8. The uncorrelated misorientation distributions for samples after one, four and twelve ECA passes. These correspond to the correlated data of Figure 5.6.

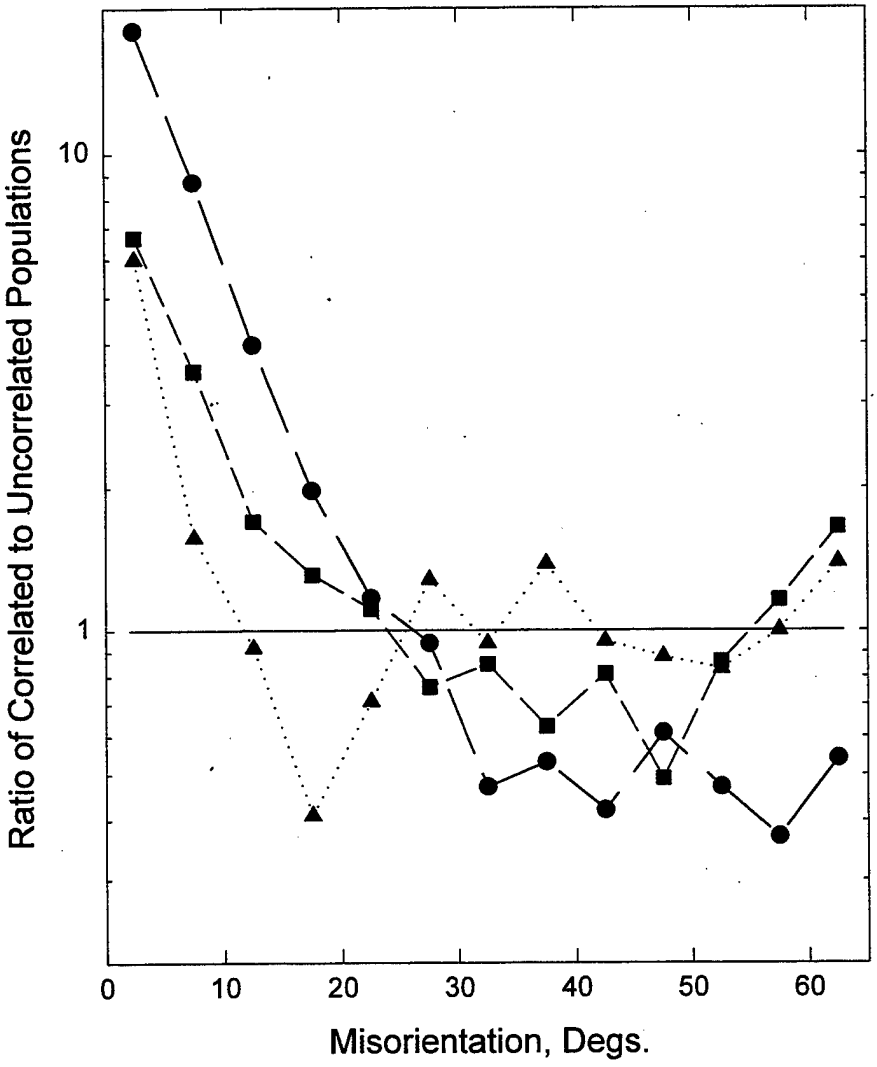

Figure 5.9. Ratio of correlated misorientation angle data to uncorrelated misorientation data. This corresponds to Figures 5.5 and 5.7.

E. DEFORMATION BANDING

Deformation banding, discussed in Chapter I, has received increasing attention for its possible role in microstructure and texture development during large-strain deformation processing of metals. Therefore, it may have a role in materials processed by the ECA pressing procedure. Such banding would take the form of orientation relationships between bands. In this study, this was investigated by examining the sequence of orientations encountered during the traverses employed to obtain the microtexture data using EBSP. Figure 5.10 illustrates six successive Kikuchi patterns during such a traverse. Similar orientations are apparent, although the data is not sufficient to draw definite conclusions regarding such banding. More data is required, e.g. through plotting of images based on specific orientations in the microstructure.

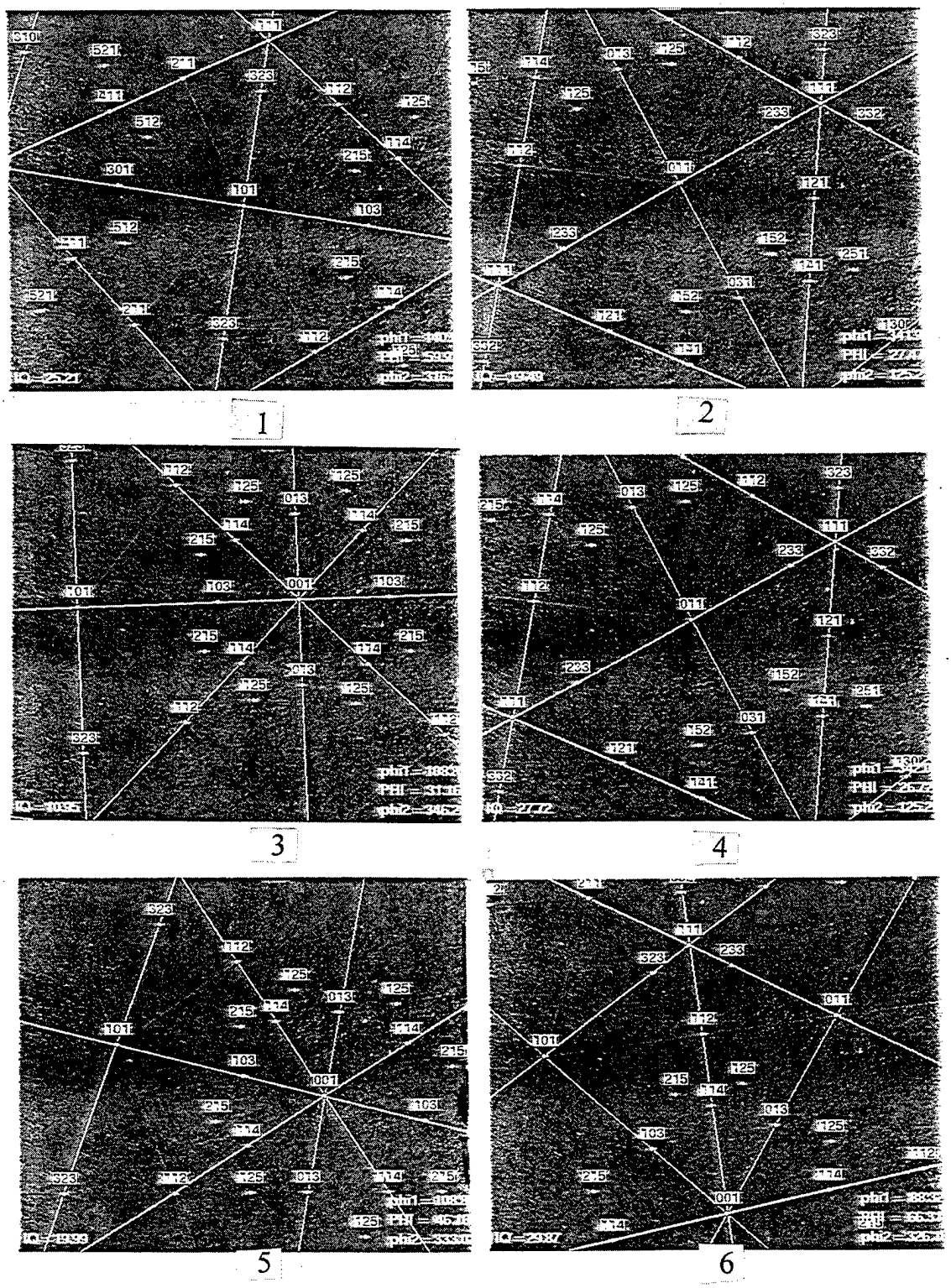

Figure 5.10. Kikuchi patterns from six adjacent grains obtained from the APR system.

V. CONCLUSIONS AND RECOMMENDATIONS

A. CONCLUSIONS

This research yielded the following conclusions: pure aluminum processed by one ECA pressing pass results in significant grain refinement, but the grain boundaries remain predominately low-angle in character. Upon successive ECA passes following route A at room temperature, further grain refinement is accompanied by a shift in the misorientation distribution toward higher boundary misorientation angles. This study has shown that processing through 12 ECA passes results in a fine, recrystallized grain structure 1.2 μm in size. After twelve passes, the texture has become random as has the misorientation distribution, resulting in a high fraction of high-angle boundaries.

B. RECOMMENDATIONS

Several areas of further investigation are recommended. These include the effect of pressing route, the effect of alloying, and the possible role of deformation banding. No conclusive results on deformation banding were obtained in this work. Complementary investigations involving both EBSD and TEM may provide the necessary data for this purpose.

This study considered only one plane of observation. Future efforts should include possible dependence on position relative to the axis of pressed samples as well as the other planes observation. The relation between grain shape and the spatial relationships between grains and grain orientations requires further investigation.

APPENDIX A. "C" PROGRAM TO OBTAIN UNCORRELATED MISORIENTATION DATA

```
load data.d
N = length(data);
k = 1;
clear NewData;
for i=1:N,
   for j=1:N,
      if(j<=i)
         % Don't write identical angles or permutations
      else
         NewData(k,:)   = data(i,:);
         NewData(k+1,:) = data(j,:);
         k = k + 2;
      end;
   end;
end;
NewData

save NewData.d NewData -ascii
```

LIST OF REFERENCES

1. Wang, J., Horita, Z., Furukawa, M., Nemoto, M., Tsenev, N., Valiev, R., Ma, Y., and Langdon, T. *Mater. Res.,* 1993, **8**, 2810.

2. Wang, J., Horita, Z., Furukawa, M., Nemoto, M., Valiev, R., and Langdon, T. *Mater. Sci. Engng.,* 1996, **A216**, 41.

3. Furukawa, M., Horita, Z., Nemoto, M., Valiev, R., and Langdon, T. *Acta Mater.,* 1996, **44**, 4619.

4. Berbon, P,. Furukawa, M., Horita, Z., Nemoto, M., Tsenev, N., Valiev, R., Ma, Y., and Langdon, T.; *Mater. Sci Forum.,* 1996, **217-222**, 1013.

5. Furukawa, M., Iwahashi, Y., Horita, Z., Nemoto, M., Tsenev, N., Valiev, R., and Langdon, T., *Acta Mater.* 1997,**45**,4751.

6. Calister, William. *Materials Science and Engineering.* 2nd ed., John Wiley and Sons, Inc., 1991.

7. Meyers, M.A. and Chawala, K.K. *Mechanical Metallurgy Principles and Applications*. Pretence-Hall, Inc.,1984.

8. Kelly, A. and Nicholson, R.B. *Strengthening Mechanisms in Crystals.* John Wiley and Sons, Inc., 1971.

9. Doherty, R.D., Hughes, D.A, Humphreys, F.J., Jonas, J.J., Jensen, D.J., Kassner, M.E., King, W.E., McNelley, T.R., McQueen, H.J., and Rollett, A.D., *Mater Sci Engng,* 1997,**A238,**219-274.

10. Chandra, T. and Hatherly, M. *Recrystallization '90, TMS, Warrendale, PA*, 1990, p.59.

11. Haasen, P. *Metall. Trans.*,1993,**24A**,1001.

12. McNelley, T.R., McMahon, M.E., and Hales, S.J., *Scripta Mater & Metall.,* 1997,**36**, 369.

13. McNelley, T.R., McMahon, M.E., *Mater Trans.,* 1997,**28A**,1879.

14. Perez-Prado, M.T., McMahon, M.E., and McNelley, T.R., in *Modeling the Mechanical Response of Structural Materials.* The Minerals, Metals and Materials Society, 1998,181.

15. Lee, C.S. and Duggan, B.J., *Acta Mater.*, 1993, **41**, 2691.

16. Kulkarni, S.S., Starke, E.A., and Kuhlmann-Wilsdorf, D., *Acta Mater.*, 1998, **46**, 5283.

17. Barrett, C.S. *Trans. Am. Inst. Min. Engrs.*, 1939,**135**,296.

18. Kaibyshev, O., Kaibyshev, R. and Salishchev, G., *Mater. Sci. Forum*, 1993, 113-115, 423.

19. Salishchev, G. A., Imayev, R. M., Imayev, V. M. and Gabdullin, N. K., *Mater Sci. Forum*, 1993, 113-115, 613.

20. Smirnova, N. A., Levit, V. I., Pilyugin, V. I., Kuznetsov, R. I., Davydova, L. S. and Sazonova, V. A., *Fiz. Metall. Metalloved.*, 1986, 61, 1170.

21. Gleiter, H., in *Deformation of Polycrystals: Mechanisms and Microstructures*, eds. N. Hansen, A. Horsewell, T. Leffers and H. Lilholt., Riso National Laboratory, Roskilde, Denmark, 1981,15.

22. Koch, C. C. and Cho, Y. S., *Nanostruct. Mater.*, 1992, **1**, 207.

23. Rigney, D. A., *Ann. Rev. Mater. Sci.*, 1988, **18**, 141.

24. Segal, V.M., Reznikov, V.I., Drobyshevskiy, A.E., and Kopylov, V.I., *Metally.* 1981,**1**;115 [English Translation: *Russian Metallurgy*, 1981,**1**,99].

25. Chokshi, A.H., Mukherjee, A.K, and T.G. Langdon, *Mater. Sci Engng.*, 1993,**10**,237-274.

26. Iwahashi, Y., Horita, Z., Nemoto, M., and Langdon, T., *Acta Mater.*, 1997, **45**, 4733.

27. Private Communication between T.G. Langdon of the University of Southern California and Department of Mechanical Engineering, Naval Postgraduate School, May 1998.

28. Private Communication between Dr. Lee of the University of Southern California and Shannon Terhune of the Naval Postgraduate School, May 1998.

29. Randle, V., Ralph, B., and Dingley, D.J., *Acta Mater.*, 1988, **36**, 267.

30. McMahon, M.E., "Grain Boundary Development in Superplastic Aluminum", PhD. Dissertation, Naval Postgraduate School, Monterey, California, December, 1996.

31. Marton, L. and Van Hove, M., *Electron Diffraction.*, Encyclopedia of Physics. Ed Lerner, R. G. and Trigg, G. L., VCH Publishers, Inc., 1991,303-305.

32. Course Literature, Orientation Imaging Academy, TexSem Laboratories Inc., Provo, Utah, 1995.

33. Cullity, B.D., *Elements of X-Ray Diffraction 2nd Edition.* Addison-Wesley Publishing Company, Inc., 1978.

34. Gibbs, M.A., Hartwig, K.T., Cornwell, L.R., Goforth, R.E., and Payzant, E.A. *Acta Mater.,* 1998, **39**, 1699.

35. Mackenzie, J.K., Biometrica, 1958,**45**,229.

36. Private Communication among Professor T. McNelley, D. Marco, and S. Terhune of the Naval Postgraduate School September 1998.

INITIAL DISTRIBUTION LIST

1. Defense Technical Information Center 2
   8725 John J. Kingman Rd., STE 0944
   Ft. Belvoir, Virginia 22060-6218

2. Dudley Knox Library 2
   Naval Postgraduate School
   411 Dyer Rd.
   Monterey, California 93943-5100

3. Naval/Mechanical Engineering, Code 34 1
   Naval Postgraduate School
   700 Dyer Rd., Bldg. 245
   Monterey, California 93943-5100

4. Department Chairman, Code ME/Mc 1
   Department of Mechanical Engineering
   Naval Postgraduate School
   700 Dyer Rd., Bldg. 245
   Monterey, California 93943-5100

5. Professor Terry R. McNelley, Code ME/Mc 5
   Department of Mechanical Engineering
   Naval Postgraduate School
   700 Dyer Rd., Bldg. 245
   Monterey, California 93943-5100

6. Professor Terence G. Langdon 2
   Departments of Materials Science and Mechanical Engineering
   University of Southern California
   Los Angeles, CA 90089-1453

7. LT Shannon Terhune 2
   26 Valley Green Drive
   Penfield, NY 14526